KINETIC DEFLECTION UNCERTAINTIES FOR REAL ASTEROID SHAPES Juliana D. Feldhacker[1], B.A. Jones[1], A. Doostan[1], D.J. Scheeres[1], J.W. McMahon[1], [1]Colorado Center for Astrodynamics Research, University of Colorado, Boulder, CO 80303 USA; juliana.feldhacker@colorado.edu

Keywords: *asteroid shape model, kinetic deflection, ANOVA*

Introduction: One proposed and technically achievable solution to the task of hazardous asteroid mitigation is the use of a projectile as a kinetic impactor to impart a change in velocity on the asteroid and thereby alter its course. A thorough understanding of the efficacy of such an approach requires comprehensive analysis of how uncertain system parameters affect the change in velocity $\Delta \boldsymbol{V}$ of the body. This quantity of interest (QOI) depends on the impact location of the projectile, the surface properties of the asteroid as represented by its β parameter, and the surface topography of the asteroid.

This paper will perform analysis on four known asteroid shapes to determine the variations expected from kinetic impactor deflection attempts due to uncertainties in β and the impact location. The analysis will first use analytic models to efficiently determine the posterior distribution of the $\Delta \boldsymbol{V}$ on the asteroid. Although a traditional Monte Carlo method could be used to complete this analysis, such an approach is computationally expensive.

Next, analysis of variance (ANOVA) parameters called Sobol' indices will be used to decompose the variation of the $\Delta \boldsymbol{V}$ into the relative individual contributions by the uncertainties in β and the impact location. While the calculation of the Sobol' indices is dependent on a Monte Carlo simulation and is therefore computationally expensive, the indices allow for a global sensitivity analysis useful when considering the asteroid body as a whole.

The first section of this paper outlines the techniques used to analytically determine the distribution of the asteroid's $\Delta \boldsymbol{V}$. Next, a definition of the Sobol' indices used for ANOVA is provided in the following section. Finally, the results of this analysis are presented as applied to the asteroids Golevka, 1950DA, Yorp, and Nereus.

Definition of the Stochastic System: The change in velocity $\Delta \boldsymbol{V} \in \mathbb{R}^3$ of an asteroid resulting from the use of a kinetic impactor is

$$\Delta \boldsymbol{V} = \gamma[\boldsymbol{V}_\infty + (\beta - 1)(\hat{\boldsymbol{n}} \cdot \boldsymbol{V}_\infty)\hat{\boldsymbol{n}}], \qquad (1)$$

where γ is the mass ratio of the impactor and asteroid, $\boldsymbol{V}_\infty \in \mathbb{R}^3$ is the velocity of the impactor with respect to the asteroid, β is a surface material property of the asteroid, and $\hat{\boldsymbol{n}} \in \mathbb{R}^3$ is the normal vector of the surface at the point of impact [1]. Thus, the stochastic nature of the $\Delta \boldsymbol{V}$ stems from uncertainties in the β and $\hat{\boldsymbol{n}}$ terms, with the values of $\hat{\boldsymbol{n}}$ defined by the realizations of the impact location. A two-dimensional local coordinate system centered at the nominal point of impact is used to map the deviation in the impact location, as shown in Figure 1, where the $\hat{\boldsymbol{u}} - \hat{\boldsymbol{w}}$ plane is perpendicular to the incoming velocity $\boldsymbol{V}_\infty$. In this study, the uncertainties in the β-parameter and in the u- and w-components of the impact location are all taken to be independently and normally distributed. The parameters defining the Gaussian distributions of the inputs can be found in Table 1.

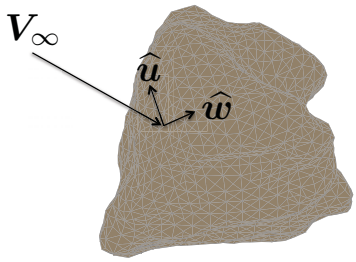

Figure 1: Triangular facet shape model for the asteroid Golevka.

Table 1: Gaussian distributions for uncertain system inputs. $\overline{R}_{ast}$ denotes the average radius of the asteroid body [2].

	Mean, μ	Standard Deviation, σ
β	2	$\frac{1}{6}$
$V_{\infty,u}$	0	$\frac{\overline{R}_{ast}}{12}$
$V_{\infty,w}$	0	$\frac{\overline{R}_{ast}}{12}$

The uncertainties in the system inputs are used to determine the distribution of the change in velocity of the asteroid resulting from impact. While the posterior distribution can be generated using a Monte Carlo simulation, this paper employs modeling techniques which allow for an analytic computation of the probability density function (pdf) of the $\Delta \boldsymbol{V}$. These techniques, which are discussed in the following sub-sections, significantly reduce the total computation time required for analysis.

Uncertainty in the Impact Location

The first technique used to reduce the computation time required to generate the pdf of the $\Delta \boldsymbol{V}$ relies on the representation of the asteroid shapes using a triangular facet shape model such as the example in Figure 2 for the asteroid Golevka. With this model, the probability of hitting any given facet can be determined analytically as a function of the incoming velocity vector, without the need for Monte Carlo simulations or computationally inefficient ray-tracking methods.

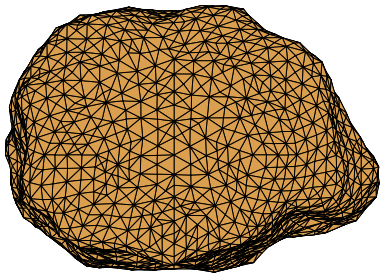

Figure 2: Triangular facet shape model for the asteroid Golevka.

The computation of the probability of impact with a given facet for a known incoming velocity vector uses a projection of the vertices of the triangular facet onto the $\hat{\boldsymbol{u}} - \hat{\boldsymbol{w}}$ plane. Because the impactor can only hit a facet for which a component of the normal vector is anti-parallel to $\boldsymbol{V}_\infty$, a projection of the normal vector for all facets onto the $\boldsymbol{V_\infty}$ vector can be used as an initial filter. Those facets which meet this criteria are then projected onto the $\hat{\boldsymbol{u}} - \hat{\boldsymbol{w}}$ plane, and the bivariate impact deviation pdf defined by the uncertainties in $V_{\infty,u}$ and $V_{\infty,w}$ (as provided in Table 1) is then integrated over the resulting domain to determine the probability of impact. The analytic solution for integrating a Gaussian distribution over a triangular domain can be found in Example 9 of [3].

In some cases, facets are partially obscured due to self-shadowing of the asteroid. The method of identifying and accounting for partially obscured facets involves determining the visibility between all facets comprising the asteroid, a process which can be completed in advance to further reduce computation time. If a facet is visible to any others, the possibility exists for a reduced probability of hitting that facet. The facet under consideration and all other visible facets are projected onto the $\hat{\boldsymbol{u}} - \hat{\boldsymbol{w}}$ plane, and the separating axis theorem [4] is used to identify any overlapping or touching triangles in this plane. For any overlapping triangles, the Sutherland-Hodgman algorithm [5] is used to solve for the polygon describing the region of overlap. Redefining the polygon as a collection of triangles using Delaunay triangulation, the sum of the integrals over these smaller triangles defines the probability over the obscured region. Figure 3 illustrates the process of solving for the overlap and the subsequent triangulation for two example triangles. The computed probability corresponding to the overlapping region is subtracted from the original probability of impacting the facet under consideration, and the procedure continues for all overlapping triangles. The total probability of impact for a given facet, then, is the integral over that facet minus the integrals over all obscured regions.

Uncertainty in β

Within a given facet, the normal vector $\hat{\boldsymbol{n}}$ remains fixed, and the $\Delta \boldsymbol{V}$ imparted on the asteroid is a linear function of the asteroid's β parameter. It follows that any uncertainties in the $\Delta \boldsymbol{V}$ are linearly related to the uncertainties in β. For a Guassian distribution in β, therefore, the $\Delta \boldsymbol{V}$ is also Gaussian. Taking the expectation of (1), the expected $\Delta \boldsymbol{V}$ from impacting a facet with the normal vector $\hat{\boldsymbol{n}}$ is

$$\mathcal{E}(\Delta \boldsymbol{V}) = \gamma[\boldsymbol{V}_\infty + (\mathcal{E}(\beta) - 1)(\hat{\boldsymbol{n}} \cdot \boldsymbol{V}_\infty)\hat{\boldsymbol{n}}]. \quad (2)$$

Similarly, its variance is given by

$$\mathcal{V}(\Delta \boldsymbol{V}) = \gamma^2[(\hat{\boldsymbol{n}} \cdot \boldsymbol{V}_\infty)^2 \hat{\boldsymbol{n}}\hat{\boldsymbol{n}}^T]V(\beta). \quad (3)$$

(2) and (3) provide a computationally efficient method of determining the distribution in the $\Delta \boldsymbol{V}$ for a single facet, yet it remains to determine a total distribution of the $\Delta \boldsymbol{V}$ for a given incoming velocity vector. The following sub-section proposes a method for calculating this distribution using the analytic solutions for the effect of uncertainty in impact location and asteroid surface properties.

Gaussian Mixture Model

With the probability of hitting a facet, as well as the distribution of $\Delta \boldsymbol{V}$ within the facet known, the method of Gaussian mixtures is well-suited for calculating the overall distribution of the asteroid's $\Delta \boldsymbol{V}$ for a given incoming trajectory. In the Gaussian mixture method, a weighted sum of N component Gaussian distributions are used to represent a pdf, such that

$$p(x) = \sum_{i=1}^{N} w_i g(x|\mu_i, \boldsymbol{\Sigma}_i), \quad (4)$$

where μ_i and Σ_i are the mean and covariance matrix of the component distributions, respectively, and the pdf p may be non-Gaussian.

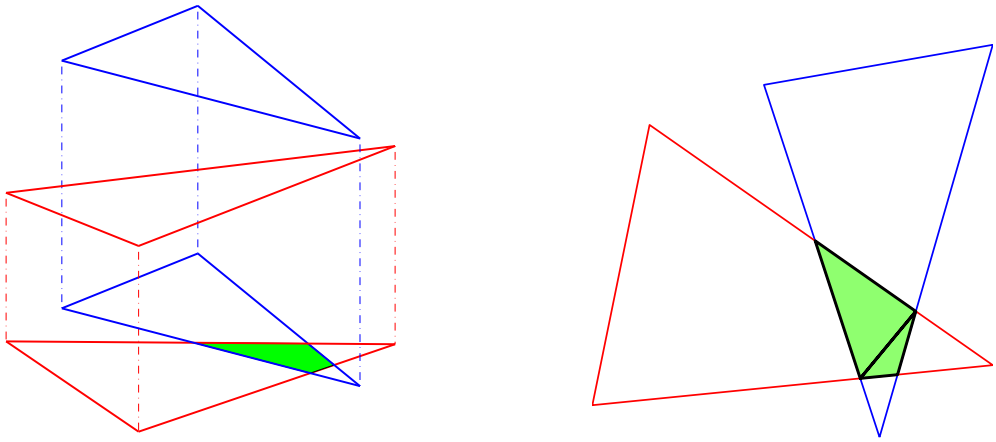

(a) Overlapping regions after projection onto two-dimensional plane

(b) Delaunay triangulation of the overlapping region

Figure 3: Illustration of the method of determining overlapping regions for two triangular facets.

For the asteroid $\Delta \boldsymbol{V}$, the component Gaussians are taken to be the $\Delta \boldsymbol{V}$ distributions for each facet of the asteroid, and the weights are taken to be the probability of hitting the facet for a given $\Delta \boldsymbol{V}_\infty$. The mean $\Delta \boldsymbol{V}$ for the specific $\boldsymbol{V}_\infty$ under consideration is therefore calculated as the weighted sum of the means,

$$[\mathcal{E}(\Delta \boldsymbol{V})]_{mix} = \sum_{i=1}^{N} w_i [\mathcal{E}(\Delta \boldsymbol{V})]_i. \tag{5}$$

The variance of the $\Delta \boldsymbol{V}$, on the other hand, must account for both the variance of the component distributions as well as the spread of the component means about the combined mean. The variance of the Gaussian sum is defined as

$$[\mathcal{V}(\Delta \boldsymbol{V})]_{mix} = \sum_{i=1}^{N} w_i [([\mathcal{E}(\Delta \boldsymbol{V})]_i - [\mathcal{E}(\Delta \boldsymbol{V})]_{mix}) * ([\mathcal{E}(\Delta \boldsymbol{V})]_i - [\mathcal{E}(\Delta \boldsymbol{V})]_{mix})^T + [\mathcal{V}(\Delta \boldsymbol{V})]_i]. \tag{6}$$

However, because the underlying $v_{\infty,u}$ and $v_{\infty,w}$ distributions used to determine the hit probabilities for each facet are Gaussian and therefore defined over an infinite domain, there exists a non-zero probability that the impactor will miss the asteroid altogether. To account for this, the weights used in the summations can normalized as

$$w_i' = \frac{w_i}{\sum_{i=1}^{N} w_i} \tag{7}$$

so that the hit probabilities sum to 1. As a result, (5) and (6) become the mean and covariance given that the impactor does in fact hit the asteroid.

By combining the three models outlined above, the distribution of the $\Delta \boldsymbol{V}$ imparted on an asteroid by a kinetic impactor with a given v_∞ can be determined purely analytically. Repeating the process for a set of nominal impact locations well-distributed about the body provides insight into the overall variation of the expected $\Delta \boldsymbol{V}$ for the asteroid.

Analysis of Variance: Analysis of variance (ANOVA) is a method which seeks to perform global sensitivity analysis by estimating the contributions of uncertainties in each input dimension to the total variance of the QOI [6]. In the context of the kinetic deflection of an asteroid, ANOVA provides a measure of the extent to which uncertainties in the β parameter and the impact location are reflected in the uncertainty of the resulting $\Delta \boldsymbol{V}$ for a given nominal impact location. This section proposes the use of a set of parameters known as the Sobol' sensitivity indices to break down the variance of the asteroid $\Delta \boldsymbol{V}$.

Sobol' Sensitivity Indices

The derivation of the Sobol' indices is based on the decomposition of the model $y = f(\boldsymbol{x})$ into summands of its input dimensions, such that

$$f(x_1, ..., x_k) = f_0 + \sum_{i=1}^{k} f_i(x_i) + \sum_{1 \le i < j \le k} f_{ij}(x_i, x_j) + \cdots + f_{1,2,...,k}(x_1, ..., x_k) \tag{8}$$

In [7], it is shown that the total variance D of the function $f(x)$ can also be decomposed into the contributions of each system input in the same way as the original function in (8), i.e.

$$D = \sum_{i=1}^{k} D_i + \sum_{1 \le i < j \le k} D_{ij} + \cdots + D_{1,2,\ldots,k}, \quad (9)$$

where

$$D_i = \mathcal{V}(\mathcal{E}(y|x_i)),$$
$$D_{ij} = \mathcal{V}(\mathcal{E}(y|x_i, x_j)) - D_i - D_j,$$

etc., for all correlated terms. The Sobol' indices are defined as the ratio of the variance in y due to dimension i to the total variance D, so that the first order indices are given by

$$S_j^1 = \frac{D_j}{D}. \quad (10)$$

Defining

$$U_j = \int \mathcal{E}^2(y|x_j = \tilde{x}_j) p_j(\tilde{x}_j) \mathrm{d}\tilde{x}_j \quad (11)$$

the variance due to each input dimension can be expressed as

$$\mathcal{V}(\mathcal{E}(y|x_j)) = U_j - \mathcal{E}^2(y), \quad (12)$$

and (10) becomes

$$S_j^1 = \frac{(U_j - \mathcal{E}^2(y))}{\mathcal{V}(y)} \quad (13)$$

Sampling-Based Calculation of the Sobol' Indices

The computation of the Sobol' indices as laid out in [8] requires a Monte Carlo simulation of n independent samples. In the empirical calculation of the indices, two sample matrices $\boldsymbol{M}_1$ and $\boldsymbol{M}_2$ of size $n \times k$ are generated,

$$\boldsymbol{M}_1 = \begin{pmatrix} x_{11} & x_{12} & \cdots & x_{1k} \\ x_{21} & x_{22} & \cdots & x_{2k} \\ \cdots & & & \\ x_{n1} & x_{n2} & \cdots & x_{nk} \end{pmatrix}$$
$$\boldsymbol{M}_2 = \begin{pmatrix} x'_{11} & x'_{12} & \cdots & x'_{1k} \\ x'_{21} & x'_{22} & \cdots & x'_{2k} \\ \cdots & & & \\ x'_{n1} & x'_{n2} & \cdots & x'_{nk} \end{pmatrix}, \quad (14)$$

where k is the number of random inputs for the system. The matrices of (14) are referred to as the "sample" and "re-sample" matrices. Another set of k matrices N_j is then generated, in which all elements except x_j are "re-sampled", i.e. x_j is taken from $\boldsymbol{M}_1$, while the remaining elements are extracted from $\boldsymbol{M}_2$, resulting in

$$\boldsymbol{N}_j = \begin{pmatrix} x'_{11} & x'_{12} & \cdots & x_{1j} & \cdots & x'_{1k} \\ x'_{21} & x'_{22} & \cdots & x_{2j} & \cdots & x'_{2k} \\ \cdots & \cdots & \cdots & \cdots & \cdots & \cdots \\ x'_{n1} & x'_{n2} & \cdots & x_{nj} & \cdots & x'_{nk} \end{pmatrix} \quad (15)$$

Function evaluations for each row of the matrices in (14) and 15 are used to calculate estimates of the parameters in (13), which are defined in [8] as

$$\hat{U}_j = \frac{1}{n-1} \sum_{r=1}^{n} f(x_{r1}, x_{r2}, ..., x_{rk}) * f(x'_{r1}, x'_{r2}, ..., x'_{r(j-1)}, x'_{rj}, x'_{r(j+1)}, ..., x'_{rk}) \quad (16)$$

and

$$\hat{\mathcal{E}}^2 = \frac{1}{n} \sum_{r=1}^{n} f(x_{r1}, x_{r2}, ..., x_{rk}) * f(x'_{r1}, x'_{r2}, ..., x'_{rk}). \quad (17)$$

Model Results: In this section, the above models are applied to the asteroids Golevka, 1950DA, Nereus, and Yorp in order to examine the relationship between asteroid shape and variation in the $\Delta \boldsymbol{V}$. For each asteroid, the expected changes in velocity are computed analytically as a function of the nominal impact location about the body, while the Sobol' indices are calculated by sampling according to the probability of hitting a facet for the random dimension of the impact location about the nominal and by sampling from the appropriate Gaussian distribution in β for each realization of the impact location.

In each case, the $\boldsymbol{V}_\infty$ of the impactor is assumed to coincide with the desired direction of the $\Delta \boldsymbol{V}$ for the asteroid, so the $\Delta \boldsymbol{V}$ is projected onto the direction parallel to $\boldsymbol{V}_\infty$ to determine the effective change in velocity in the intended direction $\Delta \boldsymbol{V}_{||}$. Further, the $\Delta \boldsymbol{V}$ is normalized by the mass fraction and the magnitude of the $\boldsymbol{V}_\infty$ to allow for comparison between asteroids.

Golevka

The statistical models are first applied to the asteroid Golevka, whose shape model can be found in Figure 4. Figure 5 depicts the $\Delta \boldsymbol{V}_{||}$ resulting from the impact, with Figure 5a providing the spatial distribution as a function of the nominal impact location and Figure 5b providing a frequency distribution as a function of the magnitude of the ΔV. The distinctive ridges of the asteroid shape are easily identifiable in Figure 5a as regions of lower $\Delta \boldsymbol{V}$. Figure 5b shows that there is significant variation in the magnitudes of $\Delta \boldsymbol{V}_{||}$ achieved

for impact locations about the body, ranging from 1.24 to 1.98 with a mean over the entire body of 1.75. Because the variance of the component distributions do not affect the mean of a Gaussian mixture (see (5)), the distribution of the expected $\Delta \boldsymbol{V}_{||}$ in Figure 5 can be attributed entirely to the topography and impact location. The 37% variation suggests, then, that the shape of the body can have a substantial influence on the effectiveness of a kinetic impactor.

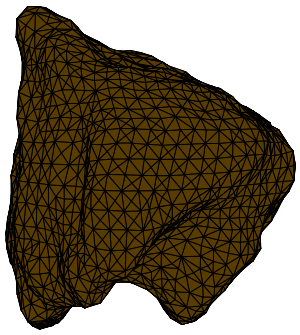

Figure 4: Triangular facet shape model for the asteroid Golevka.

Figure 6 shows the convergence of the first order Sobol' indices with increasing sample size for the parallel and perpendicular components of the $\Delta \boldsymbol{V}$, as well as its magnitude, for a single $\boldsymbol{V}_\infty$. For each sample size, 100 independent sample sets were used to generate the mean and variance of the realization of the indices. While the means of the indices are apparently independent of sample size, the variances indicate statistical convergence with increasing n. The convergence characteristics for all four asteroids were found to be very similar to those found in Figure 6, so a sample size of 1e6 was selected for subsequent analysis for all asteroids under consideration and the convergence plots have been omitted for the remaining asteroids..

The mean values in the plots to the left in Figure 6 show that the sum of the relative effects of β and the impact location is very close to one, implying that there is little to no correlated effect of the random inputs on the change in velocity. This also indicates that the S^1_β indices are complements to S^1_{uw} indices. Consequently, nearly complete information on the relative importance of the system inputs can be achieved by examining only one set of indices, allowing the number of function evaluations required for generating the indices for this application to be cut from $n(k+2)$ to $n(k+1)$ if so desired and if the slight reduction in accuracy is deemed acceptable.

Figure 7 shows the first order Sobol' indices for $\Delta \boldsymbol{V}_{||}$ as a function of the nominal impact location about Golevka for a sample size of $n = 1e6$. It is readily evident from the plots that the relative effects of the uncertainty in β portrayed in Figure 7a are complementary to those of the location uncertainty given in Figure 7b, consistent with the conclusions drawn from Figure 6. Therefore, only the set of S^1_β indices will be included for the remainder of the results.

The S^1_β indices in Figure 7a are also somewhat reminiscent of the results in Figure 5a above, easily mapped to the irregularities found in the asteroid shape model. This is a logical result, as for smooth regions of the asteroid body, the impacted facets are predominantly perpendicular to the incoming velocity vector despite any deviations in the impact location. Since β acts antiparallel to the facet normal, it also acts predominantly along the direction of $\boldsymbol{V}_\infty$ when $\hat{\boldsymbol{n}} \cdot \boldsymbol{V}_\infty$ is close to 1. Therefore, the smooth regions on the asteroid lead to the high values of the Sobol' indices indicated by the red areas in Figure 7a. Conversely, the blue areas, which represent low values of S^1_β, correspond to regions of the asteroid in which a slight deviation in the impact location can lead to large changes in the normal vector, which in turn dominates the magnitude of the resulting $\Delta \boldsymbol{V}_{||}$.

1950DA

Figure 8 provides the shape model for the asteroid 1950DA, which by examination is more nearly spherical than Golevka. The relative lack of irregularities in the shape of 1950DA produces two major differences when compared to Golevka. First, Figure 9b shows that the distribution of $\Delta \boldsymbol{V}_{||}$ ranges only from 1.54 to 1.99, smaller than the range covered by the distribution in $\Delta \boldsymbol{V}_{||}$ for Golevka. Further, a larger majority of the results are concentrated at higher values of $\Delta \boldsymbol{V}_{||}$ than was seen in the previous case, resulting in a slightly higher mean $\Delta \boldsymbol{V}_{||}$ of 1.87 over the body. Despite these differences, the magnitude varies by about 23% over the body, suggesting that the $\Delta \boldsymbol{V}_{||}$ is still sensitive to impact location and asteroid topography for 1950DA with the greatest losses occurring about the asteroid's equator.

The second effect of the differences in topography is evident in Figure 10, which indicates that the variation in $\Delta \boldsymbol{V}_{||}$ is much more predominantly dependent on uncertainties in β than was the case for Golevka. Almost all regions outside of the equator have indices $S^1_\beta > 0.5$, indicating that these areas are more sensitive to uncertainties in β than they are to uncertainties in the impact

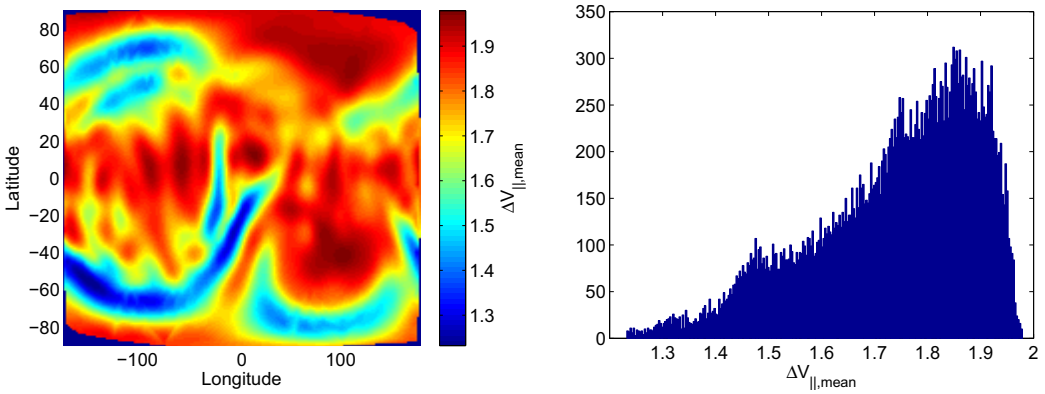

(a) Spatial distribution of $\Delta \boldsymbol{V}_{||}$

(b) Frequency distribution of $\Delta \boldsymbol{V}_{||}$

Figure 5: Variations in $\Delta \boldsymbol{V}_{||}$ due to uncertainties in the β parameter of the asteroid Golevka and in the impact location of the kinetic deflector

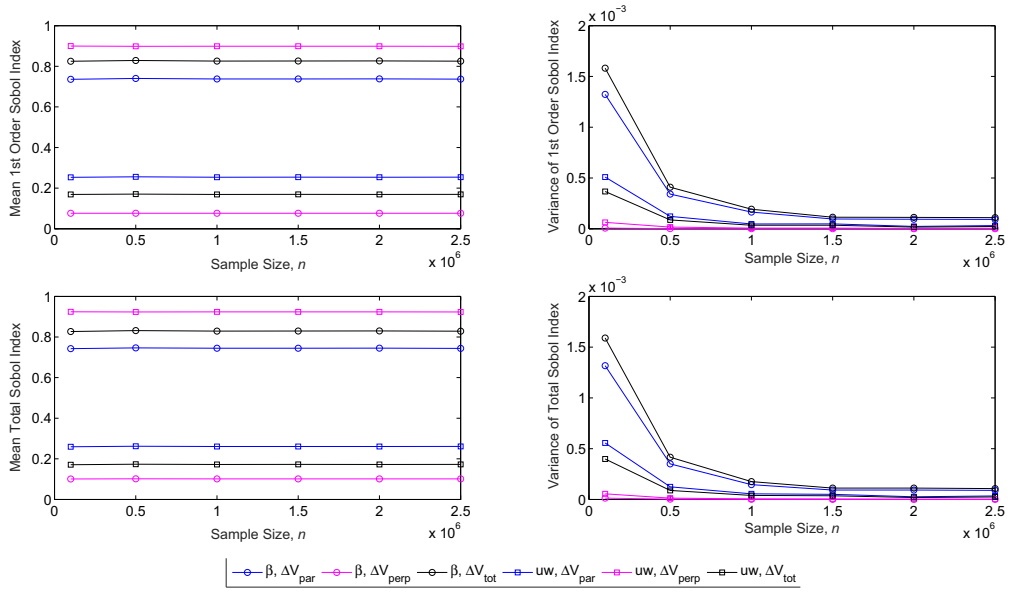

Figure 6: Mean and variance of the realizations of the first order Sobol' indices S^1_β and S^1_{uw} for 100 independent sample sets over a range of sample sizes n

location. The high dependence on β is a result of the more gradual curvature of the body in these regions.

Yorp

Figure 11 shows that the shape of the asteroid Yorp is fairly similar to that of 1950DA, and this similarity is reflected in the distribution of $\Delta \boldsymbol{V}_{||}$. In fact, the range of values seen for the $\Delta \boldsymbol{V}_{||}$ of Yorp, at 1.54-1.99, is nearly identical to the range seen for 1950DA. The overall distribution of Yorp, though, is slightly less skewed toward the larger magnitudes, for a slightly lower mean of 1.85.

As in the previous two asteroids, the plot of the S^1_β indices for Yorp depicted in Figure 13 is qualitatively similar to that of its variation in $\Delta \boldsymbol{V}_{||}$. One band in the higher latitudes, corresponding to the protrusions visible in the shape model of Figure 11, as well as a smaller band in the lower latitudes, being dominated by uncertainty in the impact position, while the remainder of the asteroid is primarily affected by uncertainties in β.

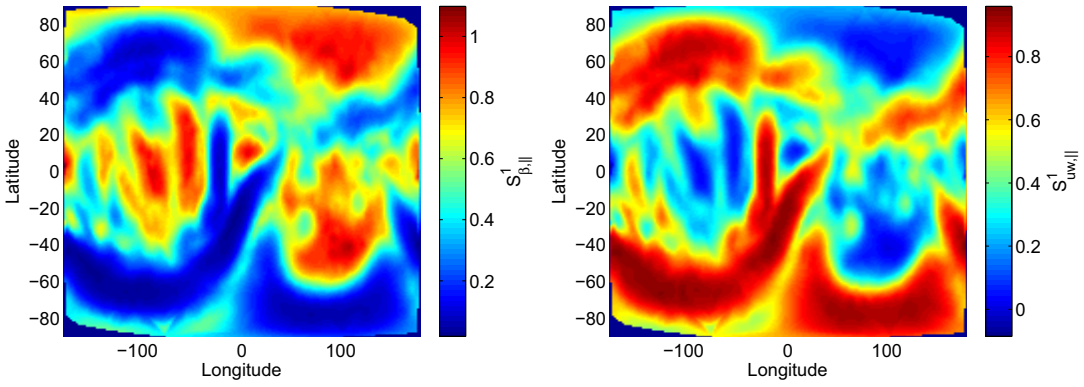

(a) S^1_β (b) S^1_{uw}

Figure 7: First order Sobol' indices for $\Delta V_{||}$ for nominal impact locations across the surface of the asteroid 1950DA

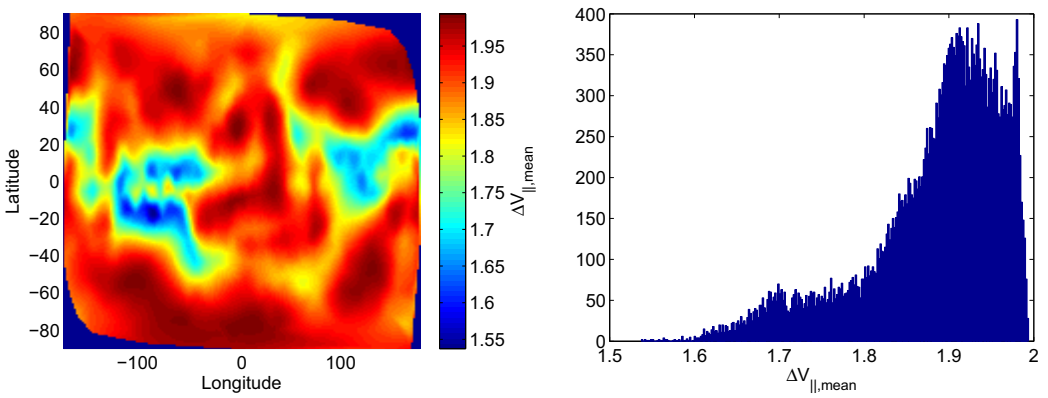

(a) Spatial distribution of $\Delta \boldsymbol{V}_{||}$ (b) Frequency distribution of $\Delta \boldsymbol{V}_{||}$

Figure 9: Variations in $\Delta V_{||}$ due to uncertainties in the β parameter of the asteroid 1950DA and in the impact location of the kinetic deflector

Nereus

The last asteroid considered in this study is Nereus, which is depicted in Figure 14. Although Nereus is more oblong than either 1950DA or Yorp, the range of $\Delta \boldsymbol{V}_{||}$ is the same as the range seen for these other two. The distribution in Figure 15b, however, is even less skewed than that of Yorp, with a mean over the body of Nereus of 1.82. In the spatial distribution of the $\Delta \boldsymbol{V}_{||}$ provided in Figure 15a, the long smooth sides of this asteroid correspond to regions of higher $\Delta \boldsymbol{V}_{||}$, while the narrow ends correspond to drops in the magnitude. This is consistent with what was seen for all three of the other asteroids regarding the rate of change in the surface topography.

Figure 16 shows that the uncertainty in the distribution of the $\Delta \boldsymbol{V}_{||}$ for Nereus is again more sensitive to variations in the β parameter about most of the body, leaving Golevka as the only one of the four asteroids to be primarily impacted by uncertainty in the impact location over a sizable portion of its surface. Thus it can be concluded that the relative influence of the uncertain input parameters is dependent not on the general shape of the asteroid, but more specifically on the presence of localized irregularities about the body, such as the ridges found on Golevka.

Conclusion: The distribution of the $\Delta \boldsymbol{V}$ resulting from the kinetic deflection of an asteroid can be efficiently determined using an analytic mapping of the uncertainty in the β parameter of the asteroid and in the

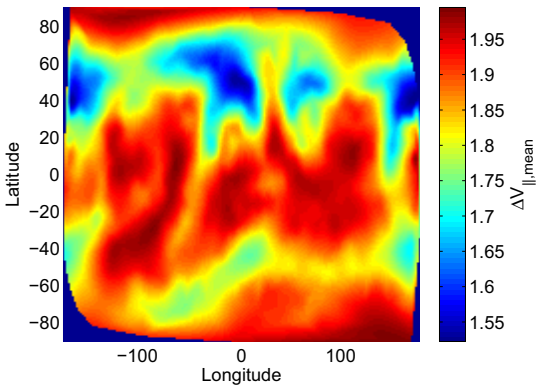

(a) Spatial distribution of $\Delta \boldsymbol{V}_{||}$

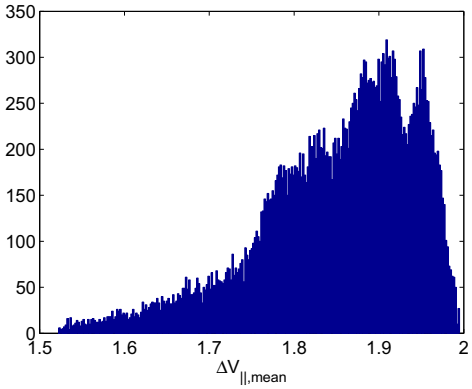

(b) Frequency distribution of $\Delta \boldsymbol{V}_{||}$

Figure 12: Variations in $\Delta \boldsymbol{V}_{||}$ due to uncertainties in the β parameter of the asteroid Yorp and in the impact location of the kinetic deflector

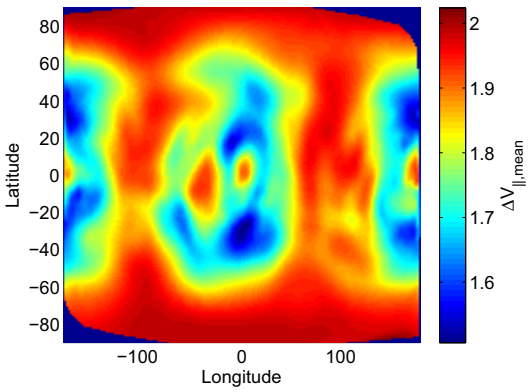

(a) Spatial distribution of $\Delta \boldsymbol{V}_{||}$

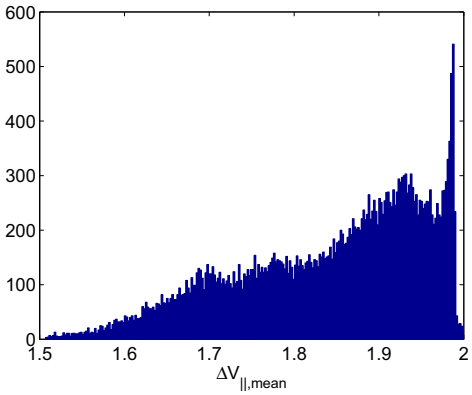

(b) Frequency distribution of $\Delta \boldsymbol{V}_{||}$

Figure 15: Variations in $\Delta \boldsymbol{V}_{||}$ due to uncertainties in the β parameter of the asteroid Nereus and in the impact location of the kinetic deflector

two-dimensional impact location. Using this technique, the deflection $\Delta \boldsymbol{V}$ is found to be highly dependent on the topography of the asteroid body under consideration. Asteroids with highly irregular shapes are more susceptible to variations in $\Delta \boldsymbol{V}_{||}$. Of the four asteroids considered in this study, 1950DA, Yorp, and Nereus all produced variations in the realized $\Delta \boldsymbol{V}$ of about 23%, while Golevka resulted in variations as high as 37%.

Sobol' indices can then be used to decompose the computed variations in $\Delta \boldsymbol{V}$ for a given $\boldsymbol{V}_\infty$ into the relative contributions by each of the system parameters. These indices show that smooth regions of the asteroid surfaces are primarily dependent on the uncertainties in β. On the other hand, uncertainties in the impact location were more influential for irregularly shaped portions of the asteroid, providing a loose correlation between regions with a high dependence on impact location uncertainty and those with greater variations in the actual $\Delta \boldsymbol{V}_{||}$. While the solution of the indices is dependent on a computationally expensive Monte Carlo simulation, they are useful in identifying where to focus efforts in terms of reducing the uncertainty in system parameters in order to achieve the greatest returns in terms of reducing uncertainty in the $\Delta \boldsymbol{V}$.

Acknowledgments: The research reported here was supported by grant NNX14AB08G from NASA's Space Technology Research Opportunities – Early Stage Innovations Program. The material is based on work of AD supported by the U.S. Department of Energy Office of Science, Office of Advanced Scientific Computing Re-

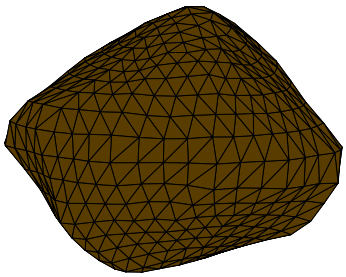

Figure 8: Triangular facet shape model for the asteroid 1950DA.

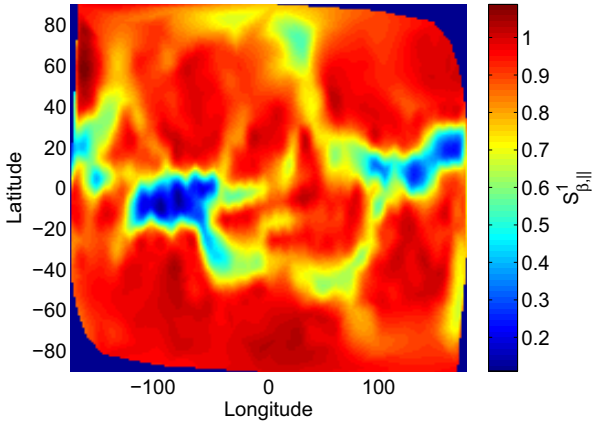

Figure 10: S^1_β for $\Delta V_{||}$ for nominal impact locations across the surface of the asteroid 1950DA.

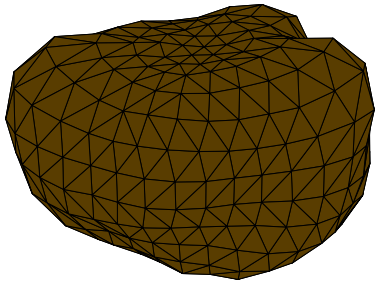

Figure 11: Triangular facet shape model for the asteroid Yorp.

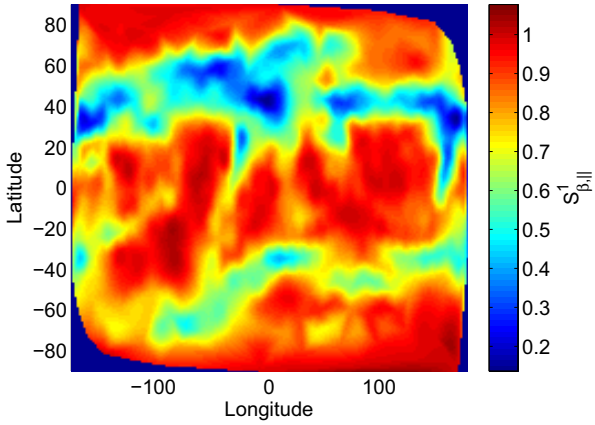

Figure 13: S^1_β for $\Delta V_{||}$ for nominal impact locations across the surface of the asteroid Yorp.

search, under Award Number DE-SC0006402. Additional funding was provided in part by the Department of Defense SMART Fellowship and Zonta International.

References: [1] K. Housen, et al. (2012) in *Lunar and Planetary Institute Science Conference Abstracts vol. 43* 2539. [2] D. J. Scheeres, et al. (2015) in *IEEE Aerospace Conference* 1–7 ISBN 9781479953806. [3] M. Abramowitz, et al. (1965) *Handbook of Mathematical Functions: with formulas, graphs, and mathematical tables* Dover Publications, New York. [4] S. Gottschalk, et al. (1996) in *Proceedings of the 23rd Annual Conference on Computer Graphics and Interactive Techniques SIGGRAPH '96* 171–180. [5] I. E. Sutherland, et al. (1974) *Communications of the ACM* 17(1):32. [6] B. Sudret (2008) *Reliability Engineering & System Safety* 93(7):964 ISSN 09518320 doi. [7] I. M. Sobol' (1993) *Mathematical Modeling and Computational Experiments* 1:407. [8] a. Saltelli, et al. (1993) *Computational Statistics & Data Analysis* 15:211 ISSN 01679473 doi.

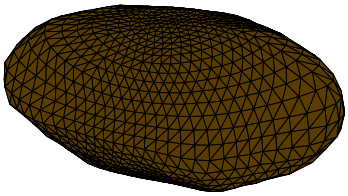

Figure 14: Triangular facet shape model for the asteroid Nereus.

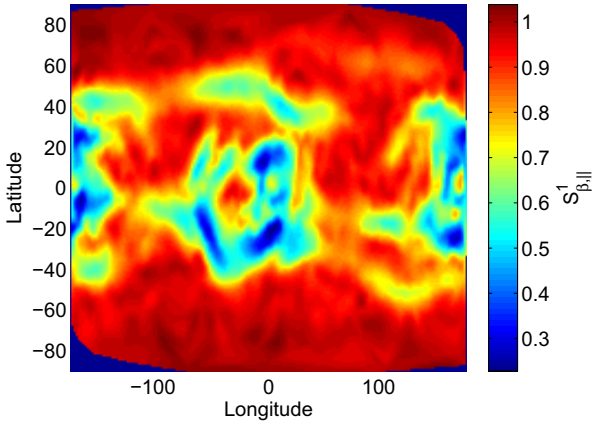

Figure 16: S^1_β for $\Delta V_{||}$ for nominal impact locations across the surface of the asteroid Nereus.